ACS APPLIED MATERIALS & INTERFACES

Research Article

www.acsami.org

Silicon Phthalocyanine Covalently Functionalized N-Doped Ultrasmall Reduced Graphene Oxide Decorated with Pt Nanoparticles for Hydrogen Evolution from Water

Jie Huang,[†,‡] Yijie Wu,[†] Dandan Wang,[†] Yufei Ma,[‡] Zongkuan Yue,[†] Yongtao Lu,[†] Mengxin Zhang,[‡] Zhijun Zhang,[‡] and Ping Yang*[,†]

[†]College of Chemistry, Chemical Engineering and Materials Science, Soochow University, Suzhou, 215123, China

[‡]Key Laboratory of Nano-Bio Interface, Division of Nanobiomedicine, Suzhou Institute of Nano-Tech and Nano-Bionics, Chinese Academy of Sciences, Suzhou 215123, China

Supporting Information

ABSTRACT: To improve the photocatalytic activity of graphene-based catalysts, silicon phthalocyanine (SiPc) covalently functionalized N-doped ultrasmall reduced graphene oxide (N-usRGO) has been synthesized through 1,3-dipolar cycloaddition of azomethine ylides. The obtained product (N-usRGO/SiPc) was characterized by transmission electron microscopy, atomic force microscopy, Fourier transform infrared spectroscopy, Raman spectra, X-ray photoelectron spectroscopy, fluorescence, and UV−vis spectroscopy. The results demonstrate that SiPc has been successfully grafted on the surface of N-usRGO. The N-usRGO/SiPc nanocomposite exhibits high light-harvesting efficiency covering a range of wavelengths from the ultraviolet to visible light. The efficient fluorescence quenching and the enhanced photocurrent response confirm that the photoinduced electron transfers from the SiPc moiety to the N-usRGO sheet. Moreover, we chose Pt nanoparticles as cocatalyst to load on N-usRGO/SiPc sheets to obtain the optimal H_2 production effect. The platinized N-usRGO/SiPc (N-usRGO/SiPc/Pt) demonstrates good hydrogen evolution performance under both UV−vis and visible light (λ>400 nm) irradiation. The apparent quantum yields are 1.3% and 0.56% at 365 and 420 nm, respectively. These results reveal that N-usRGO/SiPc/Pt nanocomposite, consolidating the advantages of SiPc, N-usRGO, and Pt NPs, can be a potential candidate for hydrogen evolution from water under UV−vis or visible light irradiation.

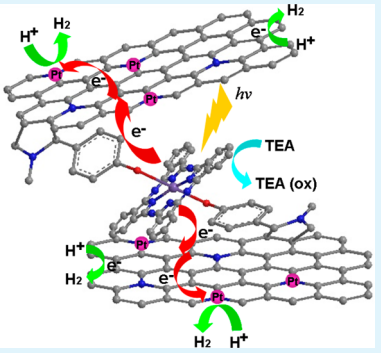

KEYWORDS: *photocatalysis, hydrogen evolution, N-doped ultrasmall graphene, silicon phthalocyanine*

1. INTRODUCTION

Hydrogen, one of the primary candidates as a future energy carrier, has recently attracted increasing attention due to the growing environmental concerns and the increasing energy demands.[1−3] One of the best ways to produce H_2 from renewable sources is water splitting under solar irradiation in the presence of photocatalysts. To achieve this goal, many semiconductors, organic/inorganic composites, and carbon-based photocatalysts have been intensively investigated.[4−6]

Graphene has attracted much attention recently because of its superior applications in the fields of electronics, optics, and catalysis.[7−10] Due to its high specific surface area, tunable band gap, and high electron mobility up to 10 000 $cm^2\ V^{-1}\ s^{-1}$, graphene is a very prospective electron acceptor and transporter to enhance photoinduced charge transfer for improving catalytic activity.[11−13] Doping graphene with other elements was found to be helpful for tailoring its electronic properties. Both electron and hole doping result in a change in the graphene lattice,[14] which in turn modulates the electronic and catalytic properties of graphene.[15−17] In addition, in order to increase the catalytic activity of graphene-based catalysts, graphene sheets are often modified with nanoparticles.[18] The heteroatoms doped in the graphene sheet may provide the initial nucleation centers for forming nanoparticles.[19] The graphene sheets can also be modified by semiconductors or photosensitizers for designing a graphene-based hybrid material. It has been proven that the hybrid materials can possess full advantages of the different components.[20−23]

Phthalocyanine (Pc) and its derivatives are promising materials for photochemical energy conversion and storage because of their excellent light-harvesting properties (the maximum around 700 nm, at which the maximum of the solar photon flux occurs).[24−29] Especially, Pcs have intense absorption ability in the red/near-infrared (IR) region of the solar spectrum, with high extinction coefficients.[30,31] Owing to their unique photochemical features, Pcs combined with semiconductors have been found to efficiently utilize the red/near-IR light of the solar radiation.[32,33]

In this work, we designed and synthesized silicon phthalocyanine (SiPc) covalently functionalized N-doped

Received: December 2, 2014
Accepted: January 23, 2015
Published: January 23, 2015

DOI: 10.1021/am508476d
ACS Appl. Mater. Interfaces 2015, 7, 3732−3741

Scheme 1. Schematic Illustration of Synthesis of N-usRGO/SiPc Nanocomposites

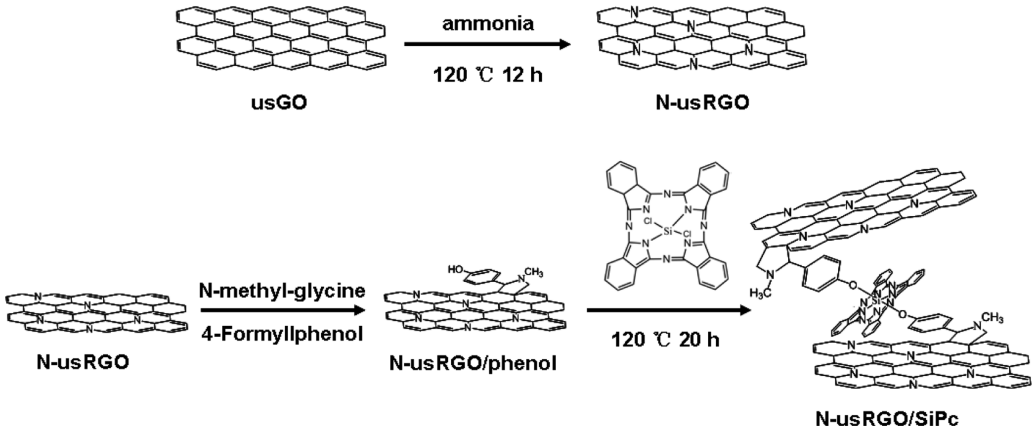

ultrasmall reduced graphene oxide (N-usRGO) through 1,3-dipolar cycloaddition of azomethine ylides. Here, N-doped ultrasmall graphene oxide is chosen as the starting material for the synthesis, because reducing the size of the GO sheets may lower the recombination probability of the photogenerated charges.[34] SiPc grafted on the N-usRGO acts as a sensitizer to harvest incident light, and the N-usRGO acts as an excellent electron acceptor and mediator to adjust electron transfer. SiPc covalently functionalized N-usRGO (N-usRGO/SiPc) exhibits much improved photocatalytic activity compared to N-usRGO, which is attributed to the nice absorption of visible light by the SiPc moiety and its covalent bonding to the usRGO sheet as well as the effective restraint of the recombination of the photoexcited electrons and holes. To improve H_2 production, Pt nanoparticles (NPs) were loaded on N-usRGO/SiPc sheets as cocatalyst by photodeposition. The platinized N-usRGO/SiPc (N-usRGO/SiPc/Pt) exhibited satisfactory photocatalytic activity under both UV−vis and visible light (λ > 400 nm) irradiation. Moreover, upon increasing the amount of the doped N in usRGO, N-usRGO/SiPc/Pt showed an enhanced photocatalytic activity. These results reveal that N-usRGO/SiPc/Pt nanocomposite with the full advantages of SiPc, N-usRGO, and Pt NPs can act as a novel candidate to produce hydrogen from water under solar light irradiation.

2. EXPERIMENTAL SECTION

2.1. Materials. Graphite, 4-formylphenol, dichlorosilicon phthalocyanine ($SiPcCl_2$), *N*-methylglycine, 1-methyl-2-pyrrolidinone (NMP), dihydrogen hexachloroplatinate(IV) hexahydrate (H_2PtCl_6), toluene, triethanolamine (TEA), and organic solvents were purchased from J&K Co. and were used without further purification.

2.2. Preparation of usGO. A yellowish black solution of usGO was obtained through a modified oxidative cutting method reported previously.[35] In brief, graphite powder (0.2 g) was cut into usGO in an oxidative mixture of H_2SO_4 (15 mL) and HNO_3 (5 mL) at 120 °C for 2 h, following by neutralization of the mixture and further dialysis against deionized water (DI water). The concentration of the used usGO solution was determined through a standard curve, which was generated by plotting the UV−vis absorption values at 230 nm against concentrations of usGO.

2.3. Preparation of N-usRGO. The N-usRGO was synthesized by chemical reduction of the usGO using ammonia as the reducing agent as well as doping agent in a water solution. In a typical procedure, 1 mL of concentrated usGO (22 mg mL^{-1}) colloidal solution was mixed with 10 mL of ammonia (28%) solution in a Teflon autoclave. Then, the reaction system was kept at 120 °C for 12 h.[36] After being cooled to room temperature, the products were dialysis against DI water for 24 h and concentrated to 10 mg mL^{-1}.

2.4. Synthesis of N-usRGO/SiPc. Scheme 1 illustrates the synthetic route of N-usRGO/SiPc nanosheets. Phenol covalently functionalized N-usRGO (N-usRGO/phenol) was prepared through 1,3-dipolar cycloaddition of azomethine ylides.[37−39] In a three-necked round-bottom flask, 2 mL of N-usRGO aqueous solution (10 mg mL^{-1}) was mixed with 98 mL of NMP, and the mixture stirred in a nitrogen atmosphere at 160 °C. After 30 min, 100 mg of *N*-methylglycine (2.2 mmol) and 125 mg of 4-formylphenol (2.1 mmol) were added (the addition of *N*-methylglycine and 4-formylphenol was repeated every 24 h four times). The temperature was kept at 160 °C with magnetic stirring. When the reaction was completed, a dark brown suspension was formed. The mixture was cooled to room temperature and dialyzed against DI water for 24 h. The obtained N-usRGO/phenol was lyophilized for future use. The N-usRGO/SiPc nanocomposites were synthesized via a substitution reaction similar to the Williamson reaction.[24,40,41] N-usRGO/phenol (20 mg) and K_2CO_3 (20 mg) were added to 60 mL of toluene, and after the mixture was stirred for 0.5 h, $SiPcCl_2$ (5.2 mg) and 18-crown-6 (4 mg) were added. The mixture was heated at reflux temperature for 20 h under a nitrogen atmosphere, which resulted in a blackish green suspension. The product was washed several times with toluene and ethanol. The final N-usRGO/SiPc powder was obtained by vacuum drying.

2.5. Preparation of Platinized N-usRGO/SiPc (N-usRGO/SiPc/Pt). The Pt NPs modified N-usRGO/SiPc (N-usRGO/SiPc/Pt) was synthesized via photodeposition of Pt NPs on N-usRGO/SiPc nanosheets.[42,43] A 50 mL portion of N-usRGO/SiPc (0.02 mg mL^{-1}) and 0.25 mL of H_2PtCl_6 (7.723×10^{-5} M) aqueous solution were added to TEA solution (10%) and mixed with magnetic stirring. The mixture was irradiated by a GY-10 xenon lamp (150 W) at room temperature for 2 h under argon, resulting in the N-usRGO/SiPc/Pt nanocomposites.

2.6. Characterization of Materials. Morphological features of the usGO nanosheets and their nanocomposites were characterized by transmission electron microscopy (TEM; Tecnai G2 F20 S-Twin) and atomic force microscopy (AFM; Veeco Dimension 3100). The absorbance and fluorescent spectra of the N-usRGO/SiPc were measured using a UV−vis spectrophotometer (UV2600, Shimadzu) and fluorescence spectrophotometer (LS 55, PerkinElmer), respectively. Fourier transform infrared (FTIR) spectra of samples (KBr pellet) were collected using a Thermo Nicolet 6700 FTIR spectrometer. Raman spectra were obtained using a confocal microprobe Raman system (HR 800) equipped with a holographic notch filter and a CCD detector. A long working distance 50× objective was used to collect the Raman scattering signal. The size of the laser spot is 1.7 mm. The excitation wavelength was 532 nm from a He−Ne laser. X-ray photoelectron spectroscopy (XPS) of materials was done with a Thermo Scientific ESCALA 250Xi XPS spectrometer. The content of Pt NPs loaded on a N-usRGO/SiPc sheet was measured by an inductively coupled plasma optical emission spectrometer (ICP-OES; Thermo Scientific iCAP 6200). ICP results of the platinized samples demonstrated that the values of Pt loading on

DOI: 10.1021/am508476d
ACS Appl. Mater. Interfaces 2015, 7, 3732−3741

N-usRGO/SiPc are in agreement with the corresponding values estimated from the starting materials (Table S1, Supporting Information).

2.7. Photoelectrochemical Measurement. The measurements of photoelectrochemical experiments were carried out on a CHI 660D potentiostat/galvanostat electrochemical analyzer in a three-electrode system that consisted of a saturated calomel electrode (SCE) as a reference electrode, a working electrode, and a platinum wire as counter electrode. The working electrode for photocurrent measurement was prepared by dipping ca. 0.5 mg of the sample on clean indium tin oxide (ITO) glass with a surface area of ca. 0.8 cm^2. The electrolyte was 0.2 M Na_2SO_4 aqueous solution. The working electrode was irradiated by a GY-10 xenon lamp (150 W) during the measurement.

The oxidation potentials and reduction potential of SiPc were measured by cyclic voltammetry using ferrocene as the standard. All the measurements were carried out in anhydrous acetonitrile containing 0.3 M lithium perchlorate ($LiClO_4$) as the supporting electrolyte. Scan rate = 0.1 V s^{-1}.

2.8. Photocatalytic Reaction. The photocatalytic reaction was run in a 50 mL quartz flask equipped with a flat optical entry window. In a typical photocatalytic experiment, 1 mg of the catalyst was dispersed in TEA (50 mL, 10%) solution. The solution was stirred continuously and irradiated by a GY-10 xenon lamp (150 W) at 298 K under atmospheric pressure. The produced gases were analyzed with an online gas chromatograph (GC1650 equipped with a thermal conductivity detector and 5 Å molecular sieve columns) using argon as the carrier gas. The standard H_2/Ar gas mixtures of the known concentrations were used for GC signal calibration. The apparent quantum efficiency (Φ_{H_2}) was measured under the same photocatalytic reaction condition except that the photocatalytic reaction was triggered at wavelengths of 365 and 420 nm as light sources. The apparent quantum efficiency Φ_{H_2} is defined by the equation

$$\Phi_{H_2} = \frac{2n_{H_2}\ (\text{mol})}{I_0\ (\text{mol s}^{-1}) \times t\ (\text{s})} \times 100\%$$

where I_0 is the number of photons per unit time. I_0 was found to be 1.09×10^{-8} mol s^{-1} and 2.46×10^{-8} mol s^{-1} for light-source wavelengths of 365 and 420 nm, respectively.

3. RESULTS AND DISCUSSION

3.1. Characterization of usGO, N-usRGO, and N-usRGO/SiPc. The yellowish brown usGO sample was obtained through a modified oxidative cutting method with a yield as high as 60%. TEM and AFM images of usGO [Figures 1A and S1 (Supporting Information)] show that the size of usGO is in the range of 3−5 nm, which is much smaller than that of GO synthesized using the modified Hummer's method.[44,45] From the high-resolution TEM (HRTEM) image (inset of Figure 1A) of the obtained usGO, the (1120) lattice fringes of graphene with a lattice parameter of 0.242 nm can be clearly observed.[35] The AFM image of usGO demonstrates its topographic morphology with ca. 0.8 nm height, corresponding to two or three graphene layers (Figure S1, Supporting Information). For the N-doped usRGO (N-usRGO), the obtained sample exhibits a size similar to that of usGO. However, as shown by Figures 1B and S1 (Supporting Information), the average thickness of N-usRGO (1.4 nm) is slightly higher than that of usGO (0.8 nm) because of the significant removal of hydroxy and epoxy groups, which results in the aggregation of N-usRGO.[46] For the SiPc covalently functionalized N-usRGO nanocomposite, the average size and thickness of N-usRGO/SiPc are about 7 nm (Figure 1C) and 2 nm (Figure 1D), respectively, which may be ascribed to the fact that one $SiPcCl_2$ molecule can conjugate with two N-usRGO sheets (Scheme 1). The energy-dispersive X-ray spectrometry

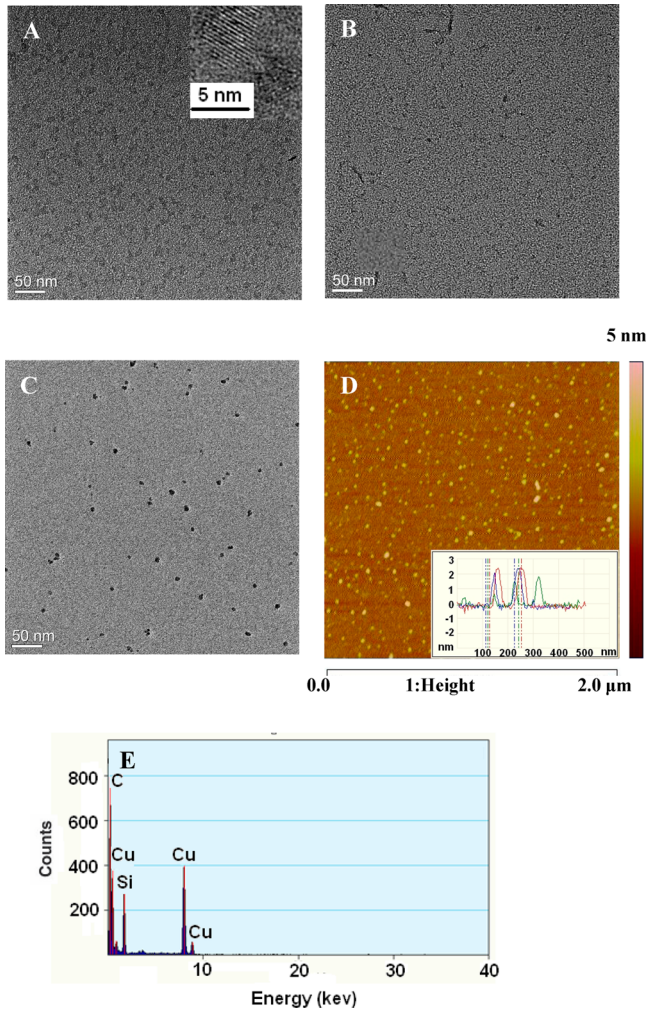

Figure 1. TEM images of usGO (A), N-usRGO (B), and N-usRGO/SiPc (C) and AFM image of N-usRGO/SiPc (D). (E) EDX pattern of the particles indicated in part C. The inset of part A is the HRTEM of usGO.

(EDX) pattern (Figure 1E) demonstrates the elementary composition of N-usRGO/SiPc. The existence of silicon confirms that SiPc has been successfully grafted on the N-usRGO sheets. The TEM image (Figure S2, Supporting Information) of platinized N-usRGO/SiPc (N-usRGO/SiPc/Pt) prepared via photodeposition shows that Pt NPs have been loaded on the N-usRGO sheet. The average size of the Pt NPs is about 2 nm.

Figure 2A presents the FTIR spectra of usGO, N-usRGO, $SiPcCl_2$, and N-usRGO/SiPc. For usGO, the peaks located at 3420 and 1353 cm^{-1} are attributed to the stretching vibration and bending vibration of O−H, respectively, and the peak at 1243 cm^{-1} is assigned to the stretching vibration of C−O group.[47] Compared to the FTIR spectrum of usGO, new peaks at 1252−1335 and 1590 cm^{-1} can be observed in the spectrum of N-usRGO, which are attributed to the N−H bending vibration and C−N stretching vibration, respectively.[47,48] The formation of the N−C bond was also confirmed by the appearance of a new peak at 1100 cm^{-1}.[48] These results, together with the fact that the intensities of the peaks corresponding to C−O and −OH groups reduced dramatically, again indicate that the nitrogen atoms have been successfully incorporated into the ultrasmall graphene nanosheets and

DOI: 10.1021/am508476d
ACS Appl. Mater. Interfaces 2015, 7, 3732−3741

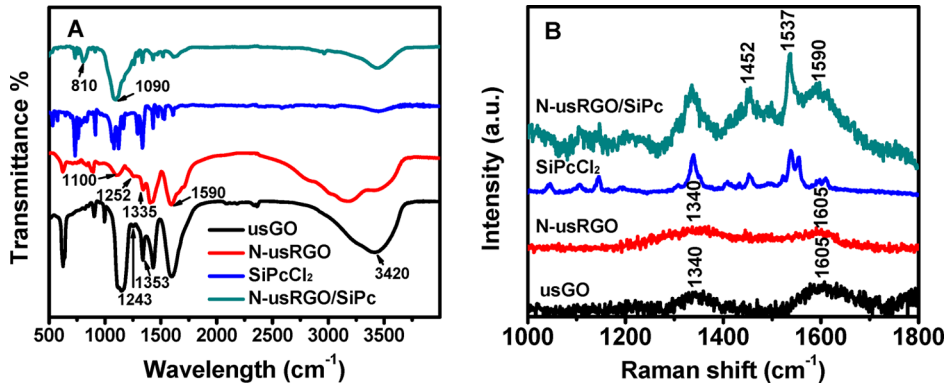

Figure 2. FTIR (A) and Raman (B) spectra of usGO, N-usRGO, $SiPcCl_2$, and N-usRGO/SiPc.

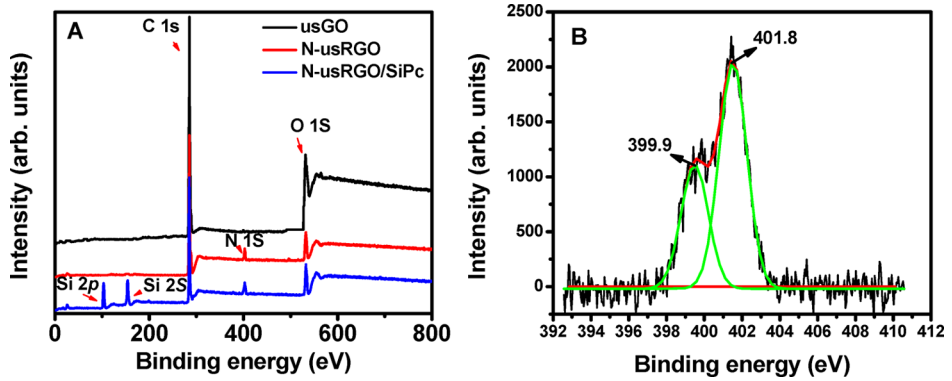

Figure 3. (A) XPS spectra of usGO, N-usRGO, and N-usRGO/SiPc, respectively. (B) High-resolution N 1s XPS spectra of N-usRGO.

usGO has been reduced to usRGO in the hydrothermal reduction process. For N-usRGO/SiPc, the absorption band in the region of 1680−1550 cm^{-1} can be appointed to the stretching vibration of the aromatic C═C and C═N bonds of the SiPc moiety.[49,50] The vibration of phenyl C−N bonds of SiPc moiety may be observed at the absorption region of 770−730 cm^{-1}.[49,50] The characteristic Si−O−C vibration is at 1090 cm^{-1}, and the weak absorption at 810 cm^{-1} is assigned to the antisymmetric O−Si−O stretching vibration.[49,50] The facts demonstrate that the SiPc are axially covalently bonded to the N-usRGO in N-usRGO/SiPc.

As shown by the Raman spectra of usGO and N-usRGO (Figure 2B), the peaks at 1340 and 1605 cm^{-1} are assigned to the D and G bands of graphene, respectively.[44,45] The D:G intensity ratio is 2.4 and 1.5 for N-usRGO and usGO, respectively, which also confirms the reduction of usGO.[51] For the N-usRGO/SiPc sample, the G band appears at 1590 cm^{-1}, which downshifts by 15 cm^{-1} compared to that of N-usRGO at 1605 cm^{-1}. This result demonstrates that an electron-donor component linked on N-usRGO successfully.[52] More notable evidence of forming N-usRGO/SiPc is that the Raman spectrum of the nanomaterial also includes peaks centered at 1452 and 1537 cm^{-1}, dovetailing the Raman peaks of $SiPcCl_2$ relating to the vibrations of pyrrolic ring vibrations.[53] These Raman spectra further prove that N-usRGO nanosheet has grafted with SiPc moiety successfully.

The XPS results shown in Figure 3A give the elemental compositions of the samples. The XPS spectrum of usGO shows the presence of carbon (285.1 eV) and oxygen (532.5 eV) elements. The high-resolution XPS spectrum of C 1s peaks can be fitted to three components, corresponding to the C−O, C═C, and O═C bonds in usGO (Figure S3, Supporting Information), which is the result of oxidation and destruction of the sp^2 atomic structure of graphite.[36] The content of O element in usGO is ca. 20 atom %, which also suggests high oxidation of usGO. The XPS spectrum of the N-usRGO sample (Figure 3A) demonstrates that the content of the oxygen element in N-usRGO is ca. 10 atom %, which is obviously lower than that of usGO, indicating the efficient reduction of usGO in the hydrothermal doping−reduction process. Furthermore, the XPS spectra of N-usRGO prepared at different temperatures (Figure S4, Supporting Information) clearly show that the doping level is about 5.7 atom % when the hydrothermal reduction temperature is kept at 120 °C, while the nitrogen-doping level increases to 7.2 atom % when the hydrothermal temperature increases to 180 °C. The fact indicates that the high temperature is beneficial for the efficient reduction and doping of usGO. In addition, the bonding configurations of nitrogen atoms in N-usRGO were confirmed by high-resolution XPS spectrum (Figure 3B). The deconvolution of the N 1s spectrum yields two peaks centered at 399.9 and 401.8 eV, which can be ascribed to the C−N−C and quaternary N, respectively,[54,55] demonstrating that N atoms have been successfully doped into the framework of graphene through the hydrothermal treatment of usGO in the presence of ammonia. For N-usRGO/SiPc, the Si 2p peak with peak widths of 2.5−3.5 eV and the Si 2s peak for Si(IV) can be observed at binding energies of 102.2−102.9 and 153 eV, respectively.[56] These results further demonstrate that SiPc has been covalently bonded on N-usRGO nanosheet successfully.

3.2. Investigation of Optical and Photoelectrochemical Properties. Figure 4A shows the UV−vis absorption spectra of usGO and N-usRGO. Compared to usGO, a new absorption peak appears at 366 nm in the spectrum of N-

DOI: 10.1021/am508476d
ACS Appl. Mater. Interfaces 2015, 7, 3732−3741

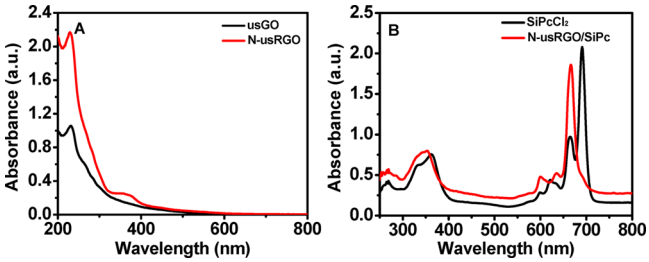

Figure 4. UV−vis spectra of (A) usGO and N-usRGO in aqueous solution and (B) $SiPcCl_2$ and N-usRGO/SiPc in THF.

usRGO, which may be appointed to the $\pi-\pi^*$ transition of pyrrole.[57] This conclusion is in accordance with the XPS results. The UV−vis absorption spectra of $SiPcCl_2$ and N-usRGO/SiPc in THF are shown in Figure 4B. $SiPcCl_2$ shows the broad B-band at 300−450 nm due to electronic transitions between molecules.[58] The Q-bands at 600−710 nm can be attributed to the allowed $\pi-\pi^*$ transition in the phthalocyanine ring.[58−60] The absorption spectrum of N-usRGO/SiPc also exhibits the same two typical electronic absorptions, indicating the presence of the SiPc moiety in the nanocomposites. The low-energy Q-band with a maxima at 665 nm of N-usRGO/SiPc shows a 27 nm blue-shift with respect to that of SiPc. This is due to the covalent attachment of SiPc to graphene, which results in some alteration of the electronic states of the phthalocyanine and the strong electronic coupling between the two π-systems of graphene and SiPc in the nanocomposite.[24,40,61] The higher energy B-band centered at 354 nm shows almost the same behavior as the Q-band, with a blue-shift and higher absorption intensity. The latter may be due to N-usRGO having a greater extinction coefficient than usGO in the UV region.[62] According to the standard curve which was measured by the UV−vis absorbance at 660 nm of $SiPcCl_2$ in THF solution, the calculated loading ration of SiPc on N-usRGO nanosheet is ca. 5%.

Figure 5 shows the fluorescence emission spectra of $SiPcCl_2$ and N-usRGO/SiPc in THF excited at 660 nm. The $SiPcCl_2$

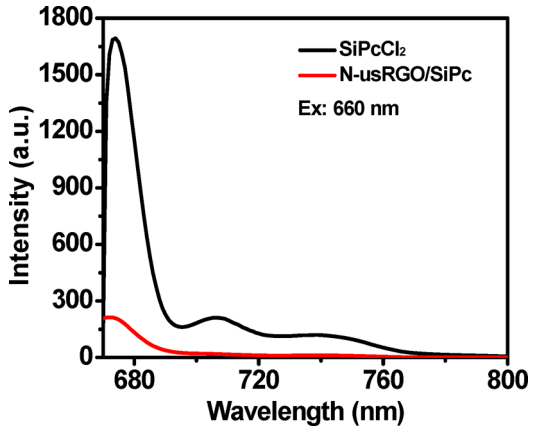

Figure 5. Fluorescence spectra of $SiPcCl_2$ and N-usRGO/SiPc in THF. The excitation wavelength was λ_{exc} = 660 nm.

sample exhibits a strong fluorescence peak at 674 nm. Compared with $SiPcCl_2$, N-usRGO/SiPc demonstrates a weak fluorescence emission at the same concentration of SiPc. The calculated quenching efficiency is 90%, suggesting efficient photoinduced electron transfer from SiPc to N-usRGO due to covalent bonding between the sensitizer moiety and N-usRGO nanosheet.[63]

Photocurrent measurements were also performed for investigating the electron transfer between the SiPc moiety and N-usRGO (Figure 6). The photocurrent response of the

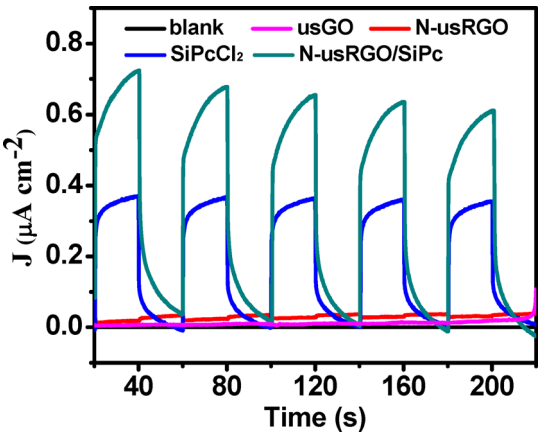

Figure 6. Photocurrent responses of ITO-electrode, usGO/ITO-electrode, N-usRGO/ITO-electrode, $SiPcCl_2$/ITO-electrode, and N-usRGO/SiPc/ITO-electrode to UV−visible light irradiation in an aqueous solution containing 0.2 M Na_2SO_4 as supporting electrolyte recorded at −0.4 V. The illumination from a 150 W xenon lamp was interrupted every 20 s.

bare ITO electrode was negligible under the performed conditions. The usGO and N-usRGO electrodes demonstrated a weak photocurrent density (ca. 0.01 and 0.03 μA cm^{-2}) due to their weak absorption of UV−visible light irradiation. However, the photocurrent density increased to 0.37 μA cm^{-2} for the $SiPcCl_2$/ITO electrode owing to the strong optical absorption of $SiPcCl_2$ and efficient photoexcited electron transfer from the sensitizer to ITO. For the N-usRGO/SiPc/ITO electrode, the steady and reproducible photocurrent response reached to ca. 0.72 μA cm^{-2}, which is ca. 2 times as high as that of the $SiPcCl_2$/ITO electrode. The significant improvement of photocurrent response of the N-usRGO/SiPc/ITO electrode may be attributed to the nice absorption of N-usRGO/SiPc in the visible-light range and efficient electron transfer from the photoexcited SiPc moiety to the covalently bonded N-usRGO nanosheet.[64,65] The photocurrent response of the N-usRGO/SiPc electrode showed significant lag after turning off the light. This phenomenon has also been observed by other researchers,[6,66,67] which could either be interpreted as the accumulated trapped charges in the electrode being detrapped slowly after turning off the light or as an intermolecular recombination of charges after illumination by light.[68]

The energy levels of SiPc are determined by cyclic voltammetry using ferrocene as the standard, and the results are presented in Figure 7. The energy levels of the LUMO (lowest unoccupied molecular orbital) and HOMO (highest occupied molecular orbital) of SiPc are defined by the equations[69]

$$E_{HOMO} = -[E^{ox} - E(Fc/Fc^+) + 4.8]\ (eV)$$

$$E_{LUMO} = -[E^{red} - E(Fc/Fc^+) + 4.8]\ (eV)$$

where $E(Fc/Fc^+)$ is the equilibrium potential of ferrocene. Thus, the measured energy levels of LUMO and HOMO of

DOI: 10.1021/am508476d
ACS Appl. Mater. Interfaces 2015, 7, 3732−3741

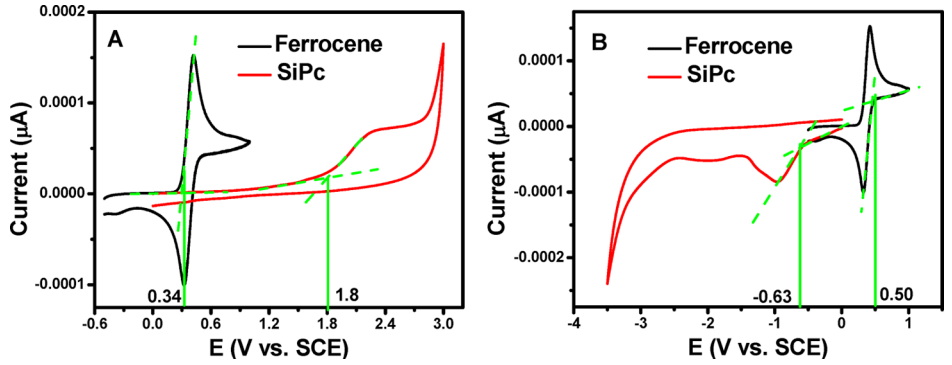

Figure 7. Oxidation potential (A) and reduction potential (B) of SiPc by cyclic voltammetry with ferrocene as the standard.

Scheme 2. (A) Energy Band Structure Diagram of Heterostructure between N-usRGO and SiPc and (B) Diagram of the Electron Transfer and Hydrogen Evolution in N-usRGO/SiPc/Pt Photocatalyst

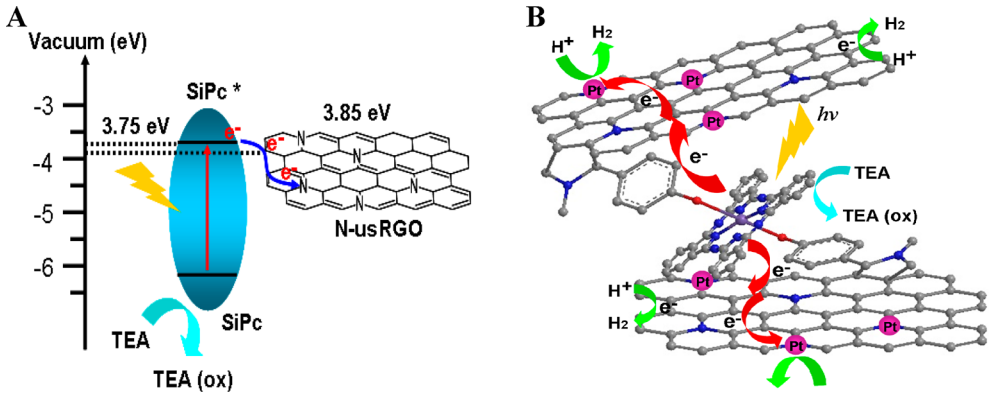

SiPc are −3.75 eV (vs vacuum) and −6.18 eV (vs vacuum), respectively. Compared with the energy level of the conduction band of N-usRGO (−3.85 eV vs vacuum),[34] we know that photoexcited electrons generated from SiPc moiety could transfer to the conduction band of N-usRGO (Scheme 2A).

3.3. Photocatalytic Hydrogen Evolution. Though many materials are capable of photocatalytically producing hydrogen from water, the overall energy conversion efficiency is still low. Suitable modification techniques such as cocatalyst loading can significantly enhance the activities of photocatalysts.[70] Here, we chose Pt NPs as cocatalyst. The photocatalytic performances of H_2 production from water over the as-prepared samples under 6 h of UV−vis light irradiation are shown in Figure 8A. The total amount of H_2 production over N-usRGO is only 0.63 μmol mg^{-1}. After the SiPc moiety grafting on the N-usRGO sheets, the total amount of H_2 production increased obviously under the same reaction conditions. This result can be attributed to the nice absorption of the visible light of SiPc moiety and its covalent connection with N-usRGO in the nanohybrid. After loading Pt NPs on N-usRGO/SiPc (Pt = 1 wt %), the amount of hydrogen production increased by 2 times compared to that of N-usRGO/SiPc. Enhancement of the photocatalysis can be attributed to Pt NPs acting as cocatalyst and reducing the overpotential in the production of H_2 from water and suppressing the fast backward reaction as well.[70−72] With the increasing of the loading amount of Pt, the evolved H_2 also increased. When the Pt content reached 5 wt %, the amount of H_2 production reached its maximum, 4.5 μmol mg^{-1}. However, higher loading of Pt over N-usRGO/SiPc does not improve the photocatalytic activity any more (Figure 8B), since the Pt loading on the N-usRGO/SiPc sheet has an optimum content for hydrogen production. For the N-usRGO/SiPc nanohybrid, the N heteroatoms doped on the RGO sheet may provide the initial nucleation sites for forming Pt NPs.[19] The intimate interaction between N-usRGO/SiPc and Pt NPs would be beneficial to the photocatalysis. Under UV−vis light irradiation, the photoexcited electrons transfer from the dye moiety to the N-usRGO surface and then subsequently are shuttled to Pt NPs deposited on N-usRGO nanosheets because of the excellent conductivity of N-usRGO and lower work function of Pt NPs. Such an ordered photoinduced electron flow would certainly promote the separation of electron−hole pairs and enhance the photoconversion efficiency.

The photocatalytic results over the as-prepared catalysts under visible light irradiation (>400 nm) are shown in Figure 8C. With 6 h of visible light irradiation, the amount of hydrogen evolved from N-usRGO/SiPc/Pt was 1.5 μmol mg^{-1}; however, N-usRGO/Pt does not produce detectable hydrogen under the same conditions because the N-usRGO nanosheet does not absorb visible light. The fact that the photocatalytic activity of N-usRGO/SiPc/Pt under visible light irradiation is relatively lower than that under UV−vis light irradiation can be interpreted to be due to the lower photoexcited energy of the visible light. Moreover, the catalytic performance of N-usRGO/SiPc/Pt under visible light irradiation mainly is owed to the red wavelength absorption of the catalyst, demonstrating the agreeable ability of the material to use the red light of the solar spectrum. The good photocatalytic performance of the nanohybrid under both UV−vis and visible light irradiation can be attributed to the SiPc moiety being covalently bonded with the N-usRGO nanosheet. The N-usRGO nanosheet here serves not only as an excellent supporting matrix for anchoring the

DOI: 10.1021/am508476d
ACS Appl. Mater. Interfaces 2015, 7, 3732−3741

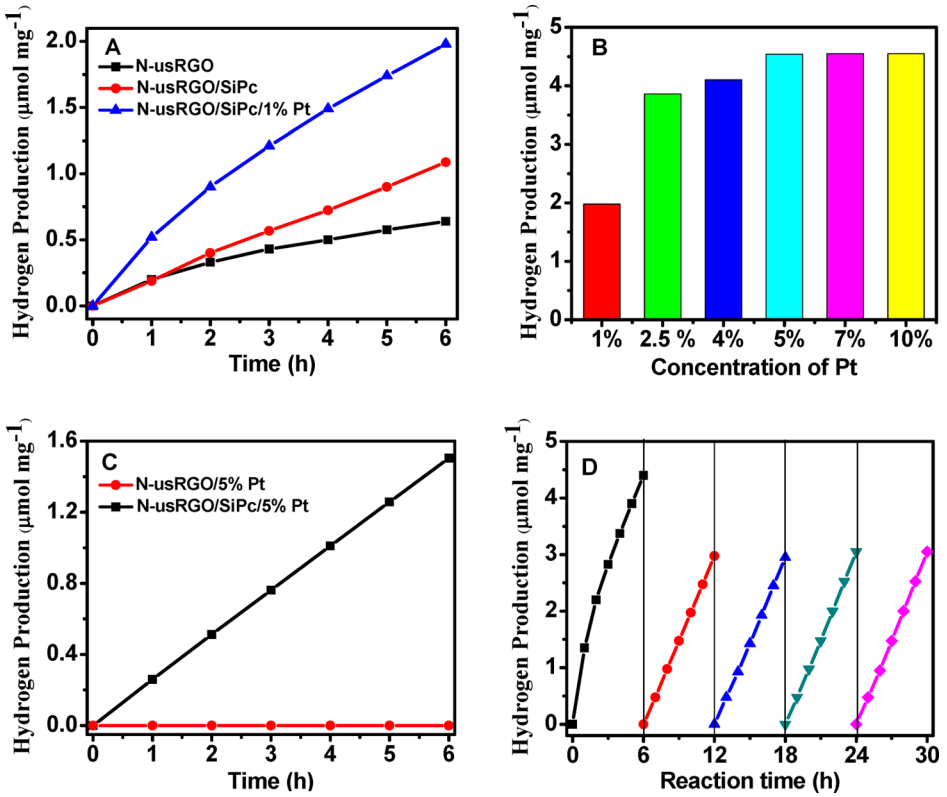

Figure 8. (A) Hydrogen production by N-usRGO/SiPc with and without Pt NPs under UV−vis irradiation. (B) Hydrogen production by N-usRGO/SiPc with different loading amount of Pt NPs (w/w). (C) Hydrogen production by N-usRGO/Pt and N-usRGO/SiPc/Pt under visible irradiation (λ > 400 nm). (D) Stability of N-usRGO/SiPc/Pt (5 wt % Pt) nanocomposite under UV−vis light irradiation. Reaction conditions: 0.5 mg of the catalyst dispersed in 50 mL of TEA (10%) solution, pH 10, T = 298 K.

sensitizer molecules and Pt cocatalyst but also as a superior electron mediator to adjust electron transfer. The calculated apparent quantum yield was 1.3% and 0.56% at 365 and 420 nm, respectively. Meanwhile, we found that the doping amount of N on usRGO sheets also influenced the hydrogen evolution. Compared to the N-usRGO prepared at 120 °C, the N-usRGO prepared at 180 °C grafting with SiPc has higher activity for hydrogen evolution (Figure S5, Supporting Information), which means that N atoms doped on N-usRGO sheets may also modulate the transfer of the photoinduced electrons, thus enhancing photocatalytic activity.[15−17]

Figure 8D shows the photocatalytic stability of N-usRGO/SiPc/Pt nanocomposite under UV−vis light irradiation. As shown by the figure, the amount of hydrogen in the first 6 h of UV−vis irradiation is 4.5 μmol mg^{-1}, and then it drops to 3.0 μmol mg^{-1} in the second run. However, the activity of the photocatalyst remains virtually unchanged in the next three runs, indicating the sufficient catalytic stability of N-usRGO/SiPc/Pt. These results suggest that this organic dye molecule covalently functionalized N-usRGO nanosheet decorated with Pt NPs is a promise candidate as a novel photocatalyst for hydrogen evolution.

The mechanism of H_2 production over N-usRGO/SiPc/Pt is illustrated in Scheme 2B. The SiPc moiety covalently bonded on the N-usRGO nanosheets acts as a light-harvesting sensitizer, absorbing light irradiation. The photoelectrons transfer from the excited sensitizers to N-usRGO nanosheet and then to Pt NPs loaded on the N-usRGO nanosheets, where the water molecules accept the electrons to form H_2. The photoexcited SiPc moiety returns back to the ground state by accepting electrons from TEA.

4. CONCLUSIONS

In summary, a novel silicon phthalocyanine covalently functionalized N-usRGO nanohybrid has been successfully synthesized and used for photocatalytic hydrogen evolution. Pt NPs acting as cocatalyst loaded on the nanohybrid were proven to enhance the photocatalytic activity. The covalent linkage between the dye moiety and N-usRGO enhances the efficiency of the photoinduced electron transfer from the sensitizer to the Pt cocatalyst via the N-usRGO nanosheet. The N heteroatoms doped on the RGO sheet not only provide the initial nucleation sites for forming Pt NPs N atoms but also act as an electron mediator to adjust photoinduced electron transfer. This study provides a new strategy for developing highly efficient carbon-based nanomaterials for photoinduced hydrogen evolution.

■ ASSOCIATED CONTENT

Supporting Information

AFM images of usGO and N-usRGO; TEM image of N-usRGO/SiPc with Pt NPs; high-resolution C 1s and O 1s XPS spectra of usGO; XPS spectra of N-usRGO prepared at 120 and 180 °C, respectively; hydrogen production by N-usRGO/SiPc/Pt that has a different amount of N; the content of Pt loaded on N-usRGO/SiPc. This material is available free of charge via the Internet at http://pubs.acs.org/.

DOI: 10.1021/am508476d
ACS Appl. Mater. Interfaces 2015, 7, 3732−3741

AUTHOR INFORMATION

Corresponding Author

*E-mail: pyang@suda.edu.cn. Tel: 86-512-65880089, Fax: 86-512-65880089.

Notes

The authors declare no competing financial interest.

ACKNOWLEDGMENTS

The authors are grateful for the financial support of this research by the National Natural Science Foundation of China (21373143), the Priority Academic Program Development of Jiangsu Higher Education Institutions (PAPD), the Project of Scientific and Technologic Infrastructure of Suzhou (SZS201207), and the Outstanding Talent Training Plan of Soochow University (5832000213).

REFERENCES

(1) Chen, Y. J.; Tian, G. H.; Ren, Z. Y.; Pan, K.; Shi, Y. H.; Wang, J. Q.; Fu, H. G. Hierarchical Core-Shell Carbon Nanofiber@$ZnIn_2S_4$ Composites for Enhanced Hydrogen Evolution Performance. *ACS Appl. Mater. Interfaces* **2014**, *6*, 13841−13849.

(2) Chaudhari, N. S.; Bhirud, A. P.; Sonawane, R. S.; Nikam, L. K.; Warule, S. S.; Rane, V. H.; Kale, B. B. Ecofriendly Hydrogen Production from Abundant Hydrogen Sulfide using Solar Light-Driven Hierarchical Nanostructured $ZnIn_2S_4$ Photocatalyst. *Green Chem.* **2011**, *13*, 2500−2506.

(3) Qu, Y. Q.; Duan, X. F. Progress, Challenge and Perspective of Heterogeneous Photocatalysts. *Chem. Soc. Rev.* **2013**, *42*, 2568−2580.

(4) Li, Y. X.; Gou, H. G.; Lu, J. J.; Wang, C. Y. A Two-Step Synthesis of $NaTaO_3$ Microspheres for Photocatalytic Water Splitting. *Int. J. Hydrogen Energy* **2014**, *39*, 13481−13485.

(5) Pany, S.; Parida, K. M. Sulfate-Anchored Hierarchical Meso-Macroporous N-Doped TiO_2: A Novel Photocatalyst for Visible Light H_2 Evolution. *ACS Sustainable Chem. Eng.* **2014**, *2*, 1429−1438.

(6) Zhang, G. G.; Wang, X. C. A Facile Synthesis of Covalent Carbon Nitride Photocatalysts by Co-Polymerization of Urea and Phenylurea for Hydrogen Evolution. *J. Catal.* **2013**, *307*, 246−253.

(7) Zhang, W. X.; Cui, J. C.; Tao, C. A.; Wu, Y. G.; Li, Z. P.; Ma, L.; Wen, Y. Q.; Li, G. T. A Strategy for Producing Pure Single-Layer Graphene Sheets Based on a Confined Self-Assembly Approach. *Angew. Chem., Int. Ed.* **2009**, *48*, 5864−5868.

(8) Li, D.; Müller, M. B.; Gilje, S.; Kaner, R. B.; Wallace, G. G. Processable Aqueous Dispersions of Graphene Nanosheets. *Nat. Nanotechnol.* **2008**, *3*, 101−105.

(9) Bag, S.; Roy, K.; Gopinath, C. S.; Raj, C. R. Facile Single-Step Synthesis of Nitrogen-Doped Reduced Graphene Oxide−Mn_3O_4 Hybrid Functional Material for the Electrocatalytic Reduction of Oxygen. *ACS Appl. Mater. Interfaces* **2014**, *6*, 2692−2699.

(10) Wang, X.; Zhi, L. J.; Müllen, K. Transparent, Conductive Graphene Electrodes for Dye-Sensitized Solar Cells. *Nano Lett.* **2008**, *8*, 323−331.

(11) Kongkanand, A.; Domínguez, R. M.; Kamat, P. V. Single Wall Carbon Nanotube Scaffolds for Photoelectrochemical Solar Cells. Capture and Transport of Photogenerated Electrons. *Nano Lett.* **2007**, *7*, 676−688.

(12) Guldi, D. M.; Rahman, G. M. A.; Sgobba, V.; Kotov, N. A.; Bonifazi, D.; Prato, M. CNT−CdTe Versatile Donor−Acceptor Nanohybrids. *J. Am. Chem. Soc.* **2006**, *128*, 2315−2323.

(13) Farrow, B.; Kamat, P. V. CdSe Quantum Dot Sensitized Solar Cells. Shuttling Electrons through Stacked Carbon Nanocups. *J. Am. Chem. Soc.* **2009**, *131*, 11124−11131.

(14) Rao, C. N. R.; Sood, A. K.; Subrahmanyam, K. S.; Govindaraj, A. Graphene: The New Two-Dimensional Nanomaterial. *Angew. Chem., Int. Ed.* **2009**, *48*, 7752−7777.

(15) Wei, D. C.; Liu, Y. Q.; Wang, Y.; Zhang, H. L.; Huang, L. P.; Yu, G. Synthesis of N-Doped Graphene by Chemical Vapor Deposition and Its Electrical Properties. *Nano Lett.* **2009**, *9*, 1752−1758.

(16) Li, X. L.; Wang, H. L.; Robinson, J. T.; Sanchez, H.; DianKov, G.; Dai, H. J. Simultaneous Nitrogen Doping and Reduction of Graphene Oxide. *J. Am. Chem. Soc.* **2009**, *131*, 15939−15944.

(17) Qu, L. T.; Liu, Y.; Baek, J. B.; Dai, L. M. Nitrogen-Doped Graphene as Efficient Metal-Free Electrocatalyst for Oxygen Reduction in Fuel Cells. *ACS Nano* **2010**, *4*, 1321−1326.

(18) Zhu, M. S.; Li, Z.; Xiao, B.; Lu, Y. T.; Du, Y. K.; Yang, P.; Wang, X. M. Surfactant Assistance in Improvement of Photocatalytic Hydrogen Production with the Porphyrin Noncovalently Functionalized Graphene Nanocomposite. *ACS Appl. Mater. Interfaces* **2013**, *5*, 1732−1740.

(19) Yin, H. J.; Tang, H. J.; Wang, D.; Gao, Y.; Tang, Z. Y. Facile Synthesis of Surfactant-Free Au Cluster/Graphene Hybrids for High-Performance Oxygen Reduction Reaction. *ACS Nano* **2012**, *6*, 8288−8297.

(20) Zhang, J.; Zhao, F.; Zhang, Z. P.; Chen, N.; Qu, L. T. Dimension-Tailored Functional Graphene Structures for Energy Conversion and Storage. *Nanoscale* **2013**, *5*, 3112−3126.

(21) Li, H. Y.; Liu, S.; Tian, J. Q.; Wang, L.; Lu, W. B.; Luo, Y. L.; Asiri, A. M.; Al-Youbi, A. O.; Sun, X. P. Ternary Nanocomposites of Porphyrin, Angular Au Nanoparticles and Reduced Graphene Oxide: Photocatalytic Synthesis and Enhanced Photocurrent Generation. *ChemCatChem* **2012**, *4*, 1079−1083.

(22) Chen, Y. Z.; Huang, Z. H.; Yue, M. B.; Kang, F. Y. Integrating Porphyrin Nanoparticles into a 2D Graphene Matrix for Free-Standing Nanohybrid Films with Enhanced Visible-Light Photocatalytic Activity. *Nanoscale* **2014**, *6*, 978−985.

(23) Khan, Z.; Chetia, T. R.; Vardhaman, A. K.; Barpuzary, D.; Sastri, C. V.; Qureshi, M. Visible Light Assisted Photocatalytic Hydrogen Generation and Organic Dye Degradation by CdS−Metal Oxide Hybrids in Presence of Graphene Oxide. *RSC Adv.* **2012**, *2*, 12122−12128.

(24) El-Khouly, M. E.; Kim, J. H.; Kay, K. Y.; Choi, C. S.; Ito, O.; Fukuzumi, S. Synthesis and Photoinduced Intramolecular Processes of Light-Harvesting Silicon Phthalocyanine−Naphthalenediimide−Fullerene Connected Systems. *Chem.—Eur. J.* **2009**, *15*, 5301−5310.

(25) Linssen, T. G.; Dürr, K.; Hanack, M.; Hirsch, A. A Green Fullerene: Synthesis and Electrochemistry of a Diels−Alder Adduct of [60]Fullerene with a Phthalocyanine. *J. Chem. Soc. Chem. Commun.* **1995**, 103−104.

(26) D'Souza, F.; Ito, O. Photoinduced Electron Transfer in Supramolecular Systems of Fullerenes Functionalized with Ligands Capable of Binding to Zinc Porphyrins and Zinc Phthalocyanines. *Coord. Chem. Rev.* **2005**, *249*, 1410−1422.

(27) Fukuzumi, S.; Ohkubo, K.; Ortiz, J.; Gutiérrez, A. M.; Fernández-Lázaro, F.; Sastre-Santos, Á. Formation of a Long-Lived Charge-Separated State of a Zinc Phthalocyanine−Perylenediimide Dyad by Complexation with Magnesium Ion. *Chem. Commun.* **2005**, *41*, 3814−3816.

(28) Xue, J. G.; Uchida, S.; Rand, B. P.; Forrest, S. R. 4.2% Efficient Organic Photovoltaic Cells with Low Series Resistances. *Appl. Phys. Lett.* **2004**, *84*, 3013−3015.

(29) Calvete, M. J. F.; Dini, D.; Flom, S. R.; Hanack, M.; Pong, R. G. S.; Shirk, J. S. Synthesis of a Bisphthalocyanine and Its Nonlinear Optical Properties. *Eur. J. Org. Chem.* **2005**, *2005*, 3499−3509.

(30) Bottari, G.; Torre, G.; Guldi, D. M.; Torres, T. Covalent and Noncovalent Phthalocyanine−Carbon Nanostructure Systems: Synthesis, Photoinduced Electron Transfer, and Application to Molecular Photovoltaics. *Chem. Rev.* **2010**, *110*, 6768−6816.

(31) Reddy, P. Y.; Giribabu, L.; Lyness, C.; Snaith, H. J.; Vijaykumar, C.; Chandrasekharam, M.; Lakshmikantam, M.; Yum, J.; Kalyanasundaram, K.; Grätzel, M.; Nazeeruddin, M. K. Efficient Sensitization of Nanocrystalline TiO_2 Films by a Near-IR-Absorbing Unsymmetrical Zinc Phthalocyanine. *Angew. Chem., Int. Ed.* **2007**, *46*, 373−376.

(32) Kim, W.; Tachikawa, T.; Majima, T.; Li, C. H.; Kim, H. J.; Choi, W. Tin-Porphyrin Sensitized TiO_2 for the Production of H_2 under Visible Light. *Energy Environ. Sci.* **2010**, *3*, 1789−1795.

DOI: 10.1021/am508476d
ACS Appl. Mater. Interfaces 2015, 7, 3732−3741

(33) Takanabe, K.; Kamata, K.; Wang, X.; Antonietti, M.; Kubota, J.; Domen, K. Photocatalytic Hydrogen Evolution on Dye-Sensitized Mesoporous Carbon Nitride Photocatalyst with Magnesium Phthalocyanine. *Phys. Chem. Chem. Phys.* **2010**, *12*, 13020−13025.
(34) Yeh, T. F.; Teng, C. Y.; Chen, S. J.; Teng, H. Nitrogen-Doped Graphene Oxide Quantum Dots as Photocatalysts for Overall Water-Splitting under Visible Light Illumination. *Adv. Mater.* **2014**, *26*, 3297−3303.
(35) Peng, J.; Gao, W.; Gupta, B. K.; Liu, Z.; Romero-Aburto, R.; Ge, L. H.; Song, L.; Alemany, L. B.; Zhan, X. B.; Gao, G. H.; Vithayathil, S. A.; Kaipparettu, B. A.; Marti, A. A.; Hayashi, T.; Zhu, J. J.; Ajayan, P. M. Graphene Quantum Dots Derived from Carbon Fibers. *Nano Lett.* **2012**, *12*, 844−849.
(36) Jiang, B. J.; Tian, C. G.; Wang, L.; Sun, L.; Chen, C.; Nong, X. Z.; Qiao, Y. J.; Fu, H. G. Highly Concentrated, Stable Nitrogen-Doped Graphene for Supercapacitors: Simultaneous Doping and Reduction. *Appl. Surf. Sci.* **2012**, *258*, 3438−3443.
(37) Quintana, M.; Spyrou, K.; Grzelczak, M.; Browne, W. R.; Rudolf, P.; Ptato, M. Functionalization of Graphene via 1,3-Dipolar Cycloaddition. *ACS Nano* **2010**, *4*, 3527−3533.
(38) Zhang, X. Y.; Hou, L. L.; Cnossen, A.; Coleman, A. C.; Ivashenko, O.; Rudolf, P.; Wees, B. J.; Browne, W. R.; Feringa, B. L. One-Pot Functionalization of Graphene with Porphyrin through Cycloaddition Reactions. *Chem.—Eur. J.* **2011**, *17*, 8957−8964.
(39) Ragoussi, M. E.; Malig, J.; Katsukis, G.; Butz, B.; Spiecker, E.; Torre, G.; Torres, T.; Guldi, D. M. Linking Photo- and Redoxactive Phthalocyanines Covalently to Graphene. *Angew. Chem., Int. Ed.* **2012**, *51*, 6421−6425.
(40) Martín-Gomis, L.; Ohkubo, K.; Fernández-Lázaro, F.; Fukuzumi, S.; Sastre-Santos, A. Synthesis and Photophysical Studies of a New Nonaggregated C60−Silicon Phthalocyanine−C60 Triad. *Org. Lett.* **2007**, *9*, 3441−3444.
(41) El-Khouly, M. E.; Kang, E. S.; Kay, K. Y.; Choi, C. S.; Aaraki, Y.; Ito, O. Silicon-Phthalocyanine-Cored Fullerene Dendrimers: Synthesis and Prolonged Charge-Separated States with Dendrimer Generations. *Chem.—Eur. J.* **2007**, *13*, 2854−2863.
(42) Li, Z.; Chen, Y. J.; Du, Y. K.; Wang, X. M.; Yang, P.; Zhen, J. W. Triphenylamine-Functionalized Graphene Decorated with Pt Nanoparticles and Its Application in Photocatalytic Hydrogen Production. *Int. J. Hydrogen Energy* **2012**, *37*, 4880−4888.
(43) Kraeutler, B.; Bard, A. J. Heterogeneous Photocatalytic Preparation of Supported Catalysts. Photodeposition of Platinum on Titanium Dioxide Powder and Other Substrates. *J. Am. Chem. Soc.* **1978**, *100*, 4317−4318.
(44) Huang, J.; Zhang, L. M.; Chen, B.; Ji, N.; Chen, F. H.; Zhang, Y.; Zhang, Z. J. Nanocomposites of Size-Controlled Gold Nanoparticles and Graphene Oxide: Formation and Applications in SERS and Catalysis. *Nanoscale* **2010**, *2*, 2733−2738.
(45) Huang, J.; Zong, C.; Shen, H.; Liu, M.; Chen, B.; Ren, B.; Zhang, Z. J. Mechanism of Cellular Uptake of Graphene Oxide Studied by Surface-Enhanced Raman Spectroscopy. *Small* **2012**, *8*, 2577−2584.
(46) Si, Y.; Samulski, E. T. Synthesis of Water Soluble Graphene. *Nano Lett.* **2008**, *8*, 1679−1682.
(47) Bose, S.; Kuila, T.; Mishra, A. K.; Kim, N. H.; Lee, J. H. Dual Role of Glycine as a Chemical Functionalizer and a Reducing Agent in the Preparation of Graphene: An Environmentally Friendly Method. *J. Mater. Chem.* **2012**, *22*, 9696−9703.
(48) Zhang, H.; Kuila, T.; Kim, N. H.; Yu, D. S.; Lee, J. H. Simultaneous Reduction, Exfoliation, and Nitrogen Doping of Graphene Oxide via a Hydrothermal Reaction for Energy Storage Electrode Materials. *Carbon* **2014**, *69*, 66−78.
(49) Orthmann, E.; Wegner, G. Catalysis of the Polycondensation of Dihydroxysiliconphthalocyanine. *Makromol. Chem. Rapid Commun.* **1986**, *7*, 243−247.
(50) Wijekoon, W. M. K. P.; Kama, S. P. Comparative Raman, Infrared and Optical Spectroscopic Studies of Thin Films of an Axially Substituted Phthalocyanine Compound. *J. Raman Spectrosc.* **1994**, *25*, 949−952.
(51) Shin, H.-J.; Kim, K. K.; Benayad, A.; Yoon, S.-M.; Park, H. K.; Jung, I.-S.; Jin, M. H.; Jeong, H.-K.; Kim, J. M.; Choi, J.-Y.; Lee, Y. H. Efficient Reduction of Graphite Oxide by Sodium Borohydride and Its Effect on Electrical Conductance. *Adv. Funct. Mater.* **2009**, *19*, 1987−1992.
(52) Chunder, A.; Pal, T.; Khondaker, S. I.; Zhai, L. Reduced Graphene Oxide/Copper Phthalocyanine Composite and Its Optoelectrical Properties. *J. Phys. Chem. C* **2010**, *114*, 15129−15135.
(53) Malig, J.; Jux, N.; Kiessling, D.; Cid, J.-J.; Vázquez, P.; Torres, T.; Guldi, D. M. Towards Tunable Graphene/Phthalocyanine−PPV Hybrid Systems. *Angew. Chem., Int. Ed.* **2011**, *50*, 3561−3565.
(54) Reddy, A. L. M.; Srivastava, A.; Gowda, S. R.; Gullapalli, H.; Dubey, M.; Ajayan, P. M. Synthesis of Nitrogen-Doped Graphene Films for Lithium Battery Application. *ACS Nano* **2010**, *4*, 6337−6342.
(55) Casanovas, J.; Ricart, J. M.; Rubio, J.; Illas, F.; Jiménez-Mateos, J. M. Origin of the Large N 1s Binding Energy in X-ray Photoelectron Spectra of Calcined Carbonaceous Materials. *J. Am. Chem. Soc.* **1996**, *118*, 8071−8076.
(56) Li, Z. Y.; Lieberman, M. XPS and SERS Study of Silicon Phthalocyanine Monolayers: Umbrella vs Octopus Design Strategies for Formation of Oriented SAMs. *Langmuir* **2001**, *17*, 4887−4894.
(57) Brédas, J. L.; Thémans, B.; André, J. M. Bipolarons in Polypyrrole Chains. *Phys. Rev. B* **1983**, *27*, 7827−7830.
(58) Torre, G. De la; Vázquez, P.; Agullo-López, F.; Torres, T. Role of Structural Factors in the Nonlinear Optical Properties of Phthalocyanines and Related Compounds. *Chem. Rev.* **2004**, *104*, 3723−3750.
(59) Biyiklioğlu, Z.; Cakir, D. Novel Axially Disubstituted Non-Aggregated Silicon Phthalocyanines. *Spectrochim. Acta, Part A* **2012**, *98*, 178−182.
(60) Tackley, D. R.; Dent, G.; Smith, W. E. Phthalocyanines: Structure and Vibrations. *Phys. Chem. Chem. Phys.* **2001**, *3*, 1419−1426.
(61) Wang, A. J.; Long, L. L.; Zhao, W.; Song, Y. L.; Humphrey, M. G.; Cifuentes, M. P.; Wu, X. Z.; Fu, Y. S.; Zhang, D. D.; Li, X. F.; Zhang, C. Increased Optical Nonlinearities of Graphene Nanohybrids Covalently Functionalized by Axially-Coordinated Porphyrins. *Carbon* **2013**, *53*, 327−338.
(62) Robinson, J. T.; Tabakman, S. M.; Liang, Y. Y.; Wang, H. L.; Casalongue, H. S.; Vinh, D.; Dai, H. J. Ultrasmall Reduced Graphene Oxide with High Near-Infrared Absorbance for Photothermal Therapy. *J. Am. Chem. Soc.* **2011**, *133*, 6825−6831.
(63) Kim, J. H.; El-khouly, M. E.; Araki, Y.; Ito, O.; Kay, K. Y. Photoinduced Processes of Subphthalocyanine−Diazobenzene−Fullerene Triad as an Efficient Excited Energy Transfer System. *Chem. Lett.* **2008**, *37*, 544−545.
(64) Wojcik, A.; Kamat, P. V. Reduced Graphene Oxide and Porphyrin. An Interactive Affair in 2-D. *ACS Nano* **2010**, *4*, 6697−6706.
(65) Zhang, X. Q.; Feng, Y. Y.; Tang, S. D.; Feng, W. Preparation of a Graphene Oxide-Phthalocyanine Hybrid through Strong $\pi-\pi$ Interactions. *Carbon* **2010**, *48*, 211−216.
(66) Konf, C.; Min, S. X.; Lu, G. X. A Novel Amorphous $CoSn_xO_y$ Decorated Graphene Nanohybrid Photocatalyst for Highly Efficient Photocatalytic Hydrogen Evolution. *Chem. Commun.* **2014**, *50*, 5037−5039.
(67) Yan, Z. P.; Yu, X. X.; Han, A.; Xu, P.; Du, P. W. Noble-Metal-Free $Ni(OH)_2$-Modified Cds/Reduced Graphene Oxide Nanocomposite with Enhanced Photocatalytic Activity for Hydrogen Production under Visible Light Irradiation. *J. Phys. Chem. C* **2014**, *118*, 22896−22903.
(68) McNeill, C. R.; Hwang, I.; Greenham, N. C. Photocurrent Transients in All-Polymer Solar Cells: Trapping and Detrapping Effects. *J. Appl. Phys.* **2009**, *106*, 024507.
(69) Xu, H.; Yu, D. H.; Liu, L. L.; Yan, P. F.; Jia, L. W.; Li, G. M.; Yue, Z. Y. Small Molecular Glasses Based on Multiposition Encapsulated Phenyl Benzimidazole Iridium(III) Complexes: Toward Efficient Solution-Processable Host-Free Electrophosphorescent Diodes. *J. Phys. Chem. B* **2010**, *114*, 141−150.

DOI: 10.1021/am508476d
ACS Appl. Mater. Interfaces 2015, 7, 3732−3741

(70) Yang, J. H.; Wang, D.; Han, H. X.; Li, C. Roles of Cocatalysts in Photocatalysis and Photoelectrocatalysis. *Acc. Chem. Res.* **2013**, *46*, 1900−1909.
(71) Li, Q.; Guo, B. D.; Yu, J. G.; Ran, J. R.; Zhang, B. H.; Yan, H. J.; Gong, J. R. Highly Efficient Visible-Light-Driven Photocatalytic Hydrogen Production of CdS-Cluster-Decorated Graphene Nanosheets. *J. Am. Chem. Soc.* **2011**, *133*, 10878−10884.
(72) Kamat, P. V. Graphene-Based Nanoarchitectures. Anchoring Semiconductor and Metal Nanoparticles on a Two-Dimensional Carbon Support. *J. Phys. Chem. Lett.* **2009**, *1*, 520−527.

DOI: 10.1021/am508476d
ACS Appl. Mater. Interfaces 2015, 7, 3732−3741